A codon-optimized Mecp2 transgene corrects breathing deficits and improves survival in a mouse model of Rett syndrome

Valerie Matagne, Yann Ehinger, Lydia Saidi, Ana Borges-Correia, Martine Barkats, Marc Bartoli, Laurent Villard, Jean-Christophe Roux

▶ **To cite this version:**

Valerie Matagne, Yann Ehinger, Lydia Saidi, Ana Borges-Correia, Martine Barkats, et al.. A codon-optimized Mecp2 transgene corrects breathing deficits and improves survival in a mouse model of Rett syndrome. Neurobiology of Disease, 2017, 99, 10.1016/j.nbd.2016.12.009 . hal-01426386

HAL Id: hal-01426386
https://amu.hal.science/hal-01426386

Submitted on 17 Jan 2023

HAL is a multi-disciplinary open access archive for the deposit and dissemination of scientific research documents, whether they are published or not. The documents may come from teaching and research institutions in France or abroad, or from public or private research centers.

L'archive ouverte pluridisciplinaire **HAL**, est destinée au dépôt et à la diffusion de documents scientifiques de niveau recherche, publiés ou non, émanant des établissements d'enseignement et de recherche français ou étrangers, des laboratoires publics ou privés.

Neurobiology of Disease 99 (2017) 1–11

Contents lists available at ScienceDirect

Neurobiology of Disease

journal homepage: www.elsevier.com/locate/ynbdi

A codon-optimized *Mecp2* transgene corrects breathing deficits and improves survival in a mouse model of Rett syndrome

Valerie Matagne [a], Yann Ehinger [a], Lydia Saidi [a], Ana Borges-Correia [a], Martine Barkats [b], Marc Bartoli [a], Laurent Villard [a], Jean-Christophe Roux [a,*]

[a] Aix Marseille Univ, INSERM, GMGF, UMR_S 910, 13385 Marseille, France
[b] Center of Research on Myology, FRE 3617 Centre National de la Recherche Scientifique, UMRS 974 INSERM, French Institute of Myology, Pierre and Marie Curie University Paris, France

ARTICLE INFO

Article history:
Received 25 July 2016
Revised 7 November 2016
Accepted 9 December 2016
Available online 11 December 2016

Keywords:
Rett syndrome
Mecp2
AAV9
Gene therapy
Animal model

ABSTRACT

Rett syndrome (RTT) is a severe X-linked neurodevelopmental disorder that is primarily caused by mutations in the methyl CpG binding protein 2 gene (*MECP2*). RTT is the second most prevalent cause of intellectual disability in girls and there is currently no cure for the disease. The finding that the deficits caused by the loss of *Mecp2* are reversible in the mouse has bolstered interest in gene therapy as a cure for RTT. In order to assess the feasibility of gene therapy in a RTT mouse model, and in keeping with translational goals, we investigated the efficacy of a self-complementary AAV9 vector expressing a codon-optimized version of *Mecp2* (AAV9-MCO) delivered via a systemic approach in early symptomatic *Mecp2*-deficient (KO) mice. Our results show that AAV9-MCO administered at a dose of 2×10^{11} viral genome (vg)/mouse was able to significantly increase survival and weight gain, and delay the occurrence of behavioral deficits. Apneas, which are one of the core RTT breathing deficits, were significantly decreased to WT levels in *Mecp2* KO mice after AAV9-MCO administration. Semi-quantitative analysis showed that AAV9-MCO administration in *Mecp2* KO mice resulted in 10 to 20% Mecp2 immunopositive cells compared to WT animals, with the highest Mecp2 expression found in midbrain regions known to regulate cardio-respiratory functions. In addition, we also found a cell autonomous increase in tyrosine hydroxylase levels in the A1C1 and A2C2 catecholaminergic Mecp2 + neurons in treated *Mecp2* KO mice, which may partly explain the beneficial effect of AAV9-MCO administration on apneas occurrence.

© 2016 Elsevier Inc. All rights reserved.

1. Introduction

Rett syndrome (RTT) is a severe X-linked neurodevelopmental disorder that is primarily caused by mutations in the methyl CpG binding protein 2 gene (*MECP2*) (Amir et al., 1999) and is the second most prevalent genetic cause of intellectual disability in girls (Hagberg, 1995; Naidu, 1997; Neul et al., 2010). It is a disease affecting not only the CNS (profound cognitive and motor deficits) but also the motor and autonomic functions (including severe breathing abnormalities). Currently, treatments are aimed at alleviating symptoms and there is no cure for RTT (Katz et al., 2012; Lombardi et al., 2015).

Mecp2 was first characterized as a transcriptional repressor (Meehan et al., 1992) but has since been involved in additional pathways such as transcriptional activation, mRNA splicing and miRNA processing (Samaco and Neul, 2011). In addition, *Mecp2* was also reported to be a genome-wide regulator of chromatin structure and a transcriptional regulator [see (Lyst and Bird, 2015) for review], which highlights the complexity of its molecular and cellular functions and explains why therapeutic approaches other than replacing *MECP2* may only partially improve RTT symptoms.

Because most *MECP2* mutations are sporadic (Amir et al., 1999), RTT can only be diagnosed after the first clinical signs appear. Therefore, any therapeutic intervention, such as gene therapy, would occur after disease onset. It was previously shown that reactivation of *Mecp2* rescued adult diseased RTT mice (Guy et al., 2007; Robinson et al., 2012) which indicates that, at least in animal models, the deficits caused by a loss of *Mecp2* are reversible. These finding suggest that gene therapy after the disease has started might still be beneficial for RTT patients.

Adeno-associated viruses (AAVs) are the vectors of choice for gene therapy because they are nonpathogenic, present a low immunogenicity and can express their transgene for a long period of time [see (Asokan et al., 2012) for review]. Among the different clades of viruses, AAV9 is of great interest for RTT gene therapy as it was shown to cross the blood brain barrier and infect brain cells after intravenous injection in both rodents and primates (Duque et al., 2009; Foust et al., 2009; Gray et al., 2011b).

* Corresponding author.
E-mail address: Jean-christophe.roux@univ-amu.fr (J.-C. Roux).
Available online on ScienceDirect (www.sciencedirect.com).

http://dx.doi.org/10.1016/j.nbd.2016.12.009
0969-9961/© 2016 Elsevier Inc. All rights reserved.

In the present study, we therefore investigated the therapeutic effect of gene therapy in a RTT mouse model, the *Mecp2* deficient (*Mecp2* KO) male mouse (Guy et al., 2001).

2. Results

2.1. The short Mecp2 promoter preferentially directs GFP expression in neurons after scAAV9 intravascular administration

In order to improve transgene expression in target cells (Mecp2 expressing cells), we used a self-complementary (sc) AAV9 vector that was previously shown to have an increased transduction efficiency over its single stranded counterpart (McCarty et al., 2001). In addition, to comply with the 2.2 kb maximum packaging capacity of the scAAV vector, we used the short mouse *Mecp2* endogenous promoter (pME) that was previously shown to preferentially drive the expression of a transgene in neuronal tissues (Adachi et al., 2005; Gray et al., 2011a).

Thirty day-old wild-type (WT) male mice were intravenously injected with a scAAV9-pME-GFP or scAAV9-CMV-GFP vector (control vector) at a dose of 5×10^9 viral genome (vg)/g BW. Three weeks after injection, the number of GFP expressing (GFP+) cells in the injected mouse brains was assessed by immunostaining (Fig. 1). A semi-quantitative analysis in 4 different brain areas showed a significantly lower number of GFP+ cells in the scAAV9-pME-GFP group compared to scAAV9-CMV-GFP (Fig.1C). This difference was mostly due to the CMV promoter directing GFP expression in non-neuronal cells as the number of GFP+ neuron like cells after injection of either vectors was similar in all brain areas, except the striatum (Fig. 1D). The neuronal specificity of the scAAV9-pME-GFP vector was confirmed by double fluorescent immunostaining using a neuron-specific marker (NeuN, Fig. 1N–P and supplemental Fig. 1). As previously reported by others (Dufour et al., 2014; Foust et al., 2009), the systemic administration of the scAAV9-CMV-GFP vector resulted in various cell co-expressing GFP and cell-specific markers such as NeuN (neuronal marker, Fig. 1H–J and supplemental Fig. 1), s100b (glial marker, supplemental Fig. 2), GFAP (astrocytic marker, supplemental Fig. 3) or CD31 (endothelial cell marker, supplemental Fig. 4). We did not observe any GFP expression in IBA1+ microglial cells in either vector-injected groups (supplemental Fig. 3).

2.2. Intravascular injection of a self-complementary AAV9 vector expressing a codon-optimized version of Mecp2 delays behavioral deficits worsening and increases survival in Mecp2 KO mice

In order to optimize the expression of Mecp2, we elected to use a codon-optimized version of the major *Mecp2* brain isoform [*Mecp2e1* (Dragich et al., 2007)] termed MCO and whose design involved the use of the most frequently used codons, the adjustment of GC content in order to prolong mRNA half-life as well as the replacement of negative cis-acting sites (Raab et al., 2010). Based on the GFP expression data obtained after injection of the control vectors (Fig. 1), we chose to increase the experimental vector dose to 2×10^{11} vg/mouse (1.6×10^{10} vg/g BW). Therefore, 30 day-old *Mecp2* KO mice were intravenously injected with a scAAV9 vector expressing MCO under the regulation of the short *Mecp2* promoter, termed AAV9-MCO. These mice (AAV9-MCO KO group) and their littermate controls (WT and/or *Mecp2* KO mice) were examined at different ages to monitor the progression of behavioral deficits (Fig. 2).

In early symptomatic, 35 day-old male mice (P35), there was a trend in decreased sensorimotor function in *Mecp2* KO mice compared to WT (accelerated rotarod test, Fig. 2A. $P = 0.06$, one-way ANOVA). We did not observe any significant difference in exploratory behavior (open field test, Fig. 2D–G) in the *Mecp2* KO group compared to the AAV9-MCO KO or WT groups. In the elevated plus maze test, P45 *Mecp2* KO mice were hypoactive (Fig. 2C) and showed decreased anxiety levels (Fig. 2B) as previously reported in another *Mecp2*-deficient mouse model (Pelka et al., 2006). This behavioral deficit was not improved by AAV9-MCO administration in *Mecp2* KO mice (Fig. 2B, C). In late symptomatic *Mecp2* KO mice (P55), we found significant alterations in sensorimotor function (Fig. 2A) as well as in exploratory behavior (Fig. 2D-G) when compared to WT mice. In AAV9-MCO treated *Mecp2* KO mice, the occurrence of these behavioral deficits seemed to be delayed as their performance on the rotarod (Fig. 2A) and in the open field (Fig. 2D-F) were not significantly different form the WT mice, except for the total vertical activity parameter that was still significantly decreased (Fig. 2G).

All mice were weighted three times a week and assessed for survival. *Mecp2* KO mice maintained on a C57Bl/6 background are lighter than their WT littermates (Guy et al., 2001) and a sudden drop in their weight curve usually marks the worsening of RTT symptoms. At the beginning of the study (P30), *Mecp2* KO mice already showed a significantly lower body weight than WT controls and there was no significant difference in weight between the treated and untreated *Mecp2* KO groups (Fig. 3A). While the *Mecp2* KO mice stopped gaining weight by P45, the AAV9-MCO KO mice kept gaining weight and were significantly heavier than the *Mecp2* KO mice at P50 and P60 (Fig. 3A). In order to better tease out the effect of AAV9-MCO on weight gain, we examined how long treated and untreated *Mecp2* KO mice kept gaining weight (age at peak weight) and recorded their maximum weight (Wmax). We found that AAV9-MCO KO mice kept gaining weight significantly longer than the untreated *Mecp2* KO ones (age at peak weight, 83d ± 9.1d vs 54.1d ± 4.3d, $P < 0.021$, AAV9-MCO KO vs KO by Mann-Whitney U statistics test). In addition, treated *Mecp2* KO mice reached a Wmax that was significantly higher than that of untreated *Mecp2* KO (Fig. 3A).

We also observed a significant increase in the survival median period in the AAV9-MCO KO group compared to the untreated one (99d vs 56d, respectively, $P = 0.014$, Kaplan-Meier survival analysis, Fig. 3B).

2.3. AAV9-MCO administration to Mecp2 KO mice results in low but widespread Mecp2 expression following a rostro-caudal gradient

After AAV9-MCO injection, Mecp2 expressing (Mecp2+) cells were identified by immunostaining and subsequently quantified by automated counting using the ImageJ *particle analyzing tool* (Fig. 4). As expected, we did not find any Mecp2 expression in the brains of *Mecp2* KO mice (4D, G and 4 J, M). In forebrain regions of AAV9-MCO KO mice, the number of Mecp2+ cells was around 10% of the WT number while it doubled in hindbrain regions (Fig. 4C). As seen with the scAAV9-pME-GFP construct (Fig. 1N–P), almost all Mecp2+ cells in the AAV9-MCO KO mice were neurons co-expressing NeuN (Fig. 4H, N, supplemental Fig. 5). While we could not find any Mecp2+ GFAP+ astrocyte (supplemental Fig. 6A–L), we did find Mecp2+ cells at the gliovascular interface (supplemental Fig. 6a–l).

2.4. AAV9-MCO administration to Mecp2 KO mice prevents the occurrence of apneas and increases TH levels in a cell autonomous manner

Breathing dysfunctions are common in RTT patients, as well as in RTT mouse model (Katz et al., 2009; Viemari et al., 2005), and may be responsible for a quarter of the unexplained sudden death observed in RTT patients (Julu et al., 1997; Kerr et al., 1997). In order to assess the effect of AAV9-MCO on breathing, whole body plethysmography was used to determine breathing parameters in symptomatic *Mecp2* KO mice (P45). As previously reported (Roux et al., 2007; Viemari et al., 2005), *Mecp2* KO mice had a significantly higher number of apneas when compared to WT mice and this abnormality was normalized by AAV9-MCO injection as soon as 15 days post-injection (P45) and seemed to last at least until P80 (Fig. 5). Among the other breathing parameters recorded at P45 (Table 1), the number of hypoventilation, the mean frequency and the variability were found to be significantly different in *Mecp2* KO compared to WT mice. In the AAV9-MCO KO group,

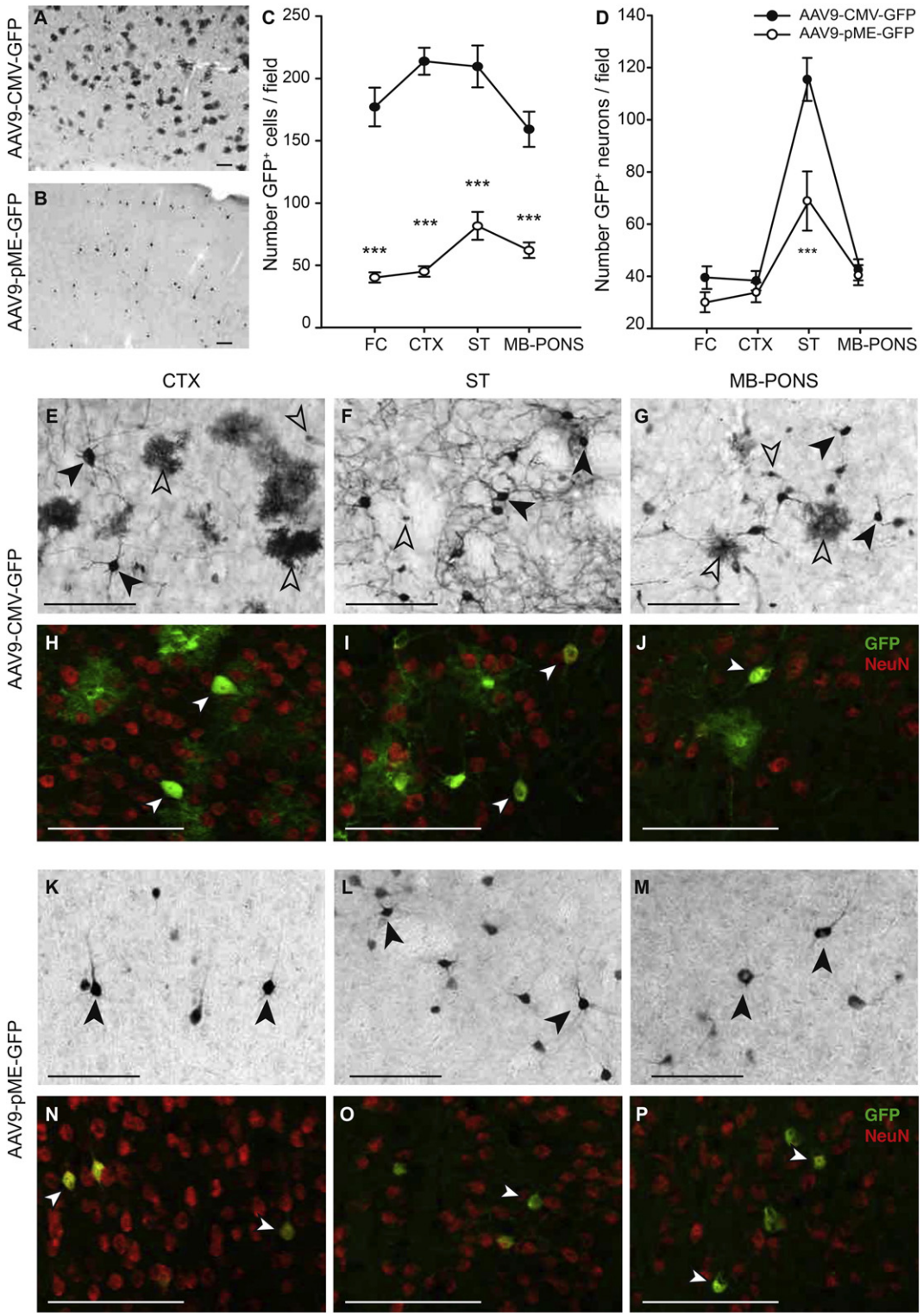

Fig. 1. The short endogenous *Mecp2* promoter preferentially directs brain GFP expression in neurons. Thirty-day old WT male mice were intravenously administered with the scAAV9-CMV-GFP ($n = 6$, except in CTX for which $n = 7$) or the scAAV9-pME-GFP vector ($n = 7$) at a dose of 5×10^9 vg/g BW and GFP expressing (GFP+) cells were identified by immunostaining 3 weeks post-injection. Pictures (A, B) were taken at 10× magnification and GFP+ cells were manually counted and grouped into neuronal and non-neuronal cells based on cellular morphology. Four fields/brain region were analyzed. There were significantly more GFP+ cells in the brains of scAAV9-CMV-GFP mouse compared to the scAAV9-pME-GFP ones (C). This difference was mostly due to higher numbers of non-neuronal GFP+ cells as the number of GFP+ neurons counted in both groups were similar, except in the striatal region (D). Higher magnification pictures showing representative GFP+ neuronal (presence of axon and/or dendrites, closed arrowheads) and non-neuronal cells (open arrowheads) found in 3 different brain areas. The expression of the NeuN neuronal marker in GFP+ cells (white arrowheads) was used to verify the identity of neuronal cells in both scAAV9-CMV-GFP (H-J) and scAAV9-pME-GFP (N-P) mouse brain by double immunostaining. FC: frontal cortex, CTX: motor cortex, ST: striatum, MB-PONS: midbrain-pons region. Data are expressed as mean ± SEM. $^{**}P < 0.01$;$^{***}P < 0.001$, Mann-Whitney *U* test, scAAV9-CMV-GFP vs scAAV9-pME-GFP. Scale bar = 100 μm.

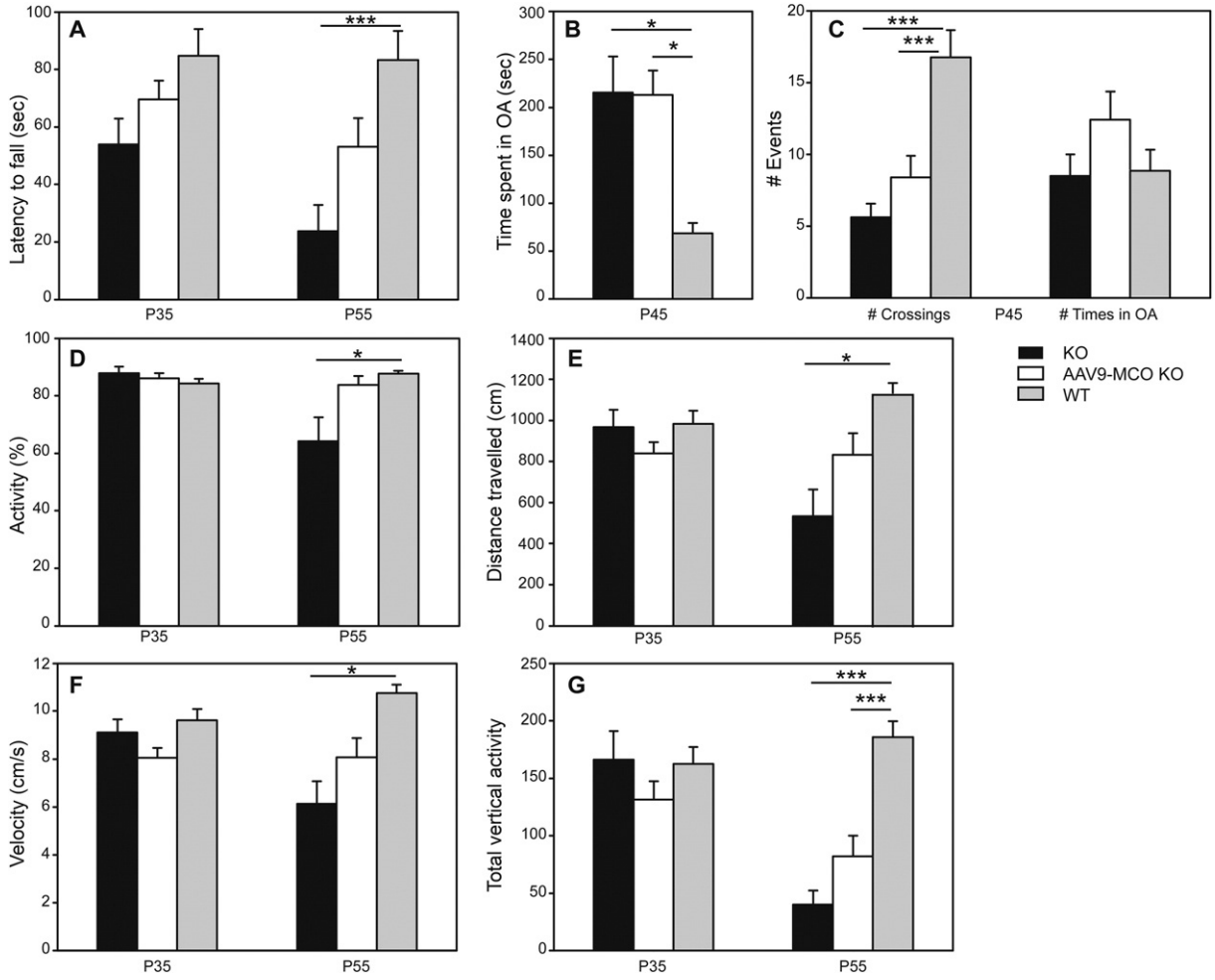

Fig. 2. AAV9-MCO administration to juvenile *Mecp2* KO mice delays RTT symptoms progression. Thirty-day old *Mecp2* KO mice were intravenously administered with AAV9-MCO (1.6×10^{10} vg/g BW) and subsequently assessed for behavioral performances together with their WT and *Mecp2* KO untreated (KO) littermate controls at P35 (n: KO = 8, AAV9-MCO = 11, WT = 13), P45 (n: KO = 8, AAV9-MCO = 10, WT = 13) and P55 (n: KO = 8, AAV9-MCO = 9, WT = 12). Vertical bars are mean + SEM. A: Sensorimotor function was assessed by the accelerated rotarod test. At P35, there was a trend in decreased sensorimotor function in *Mecp2* KO mice compared to WT ($P = 0.06$, 1-way ANOVA), and this difference was significant at P55 ($^{*}P < 0.05$, Kruskal-Wallis test with Dunn's multiple comparison). Treated AAV9-MCO KO mice showed slightly better sensorimotor function over KO mice. B,C: Anxiety-related behavior was examined in the elevated plus maze at P45. Compared to the WT mice, KO mice showed lower anxiety-related behavior and decreased activity as they spent more time in the open arms of the maze (B) and less often crossed the central platform (C), respectively. AAV9-MCO administration to *Mecp2* KO mice did not rescue these behavioral abnormalities ($^{***}P < 0.001$, 1-way ANOVA with Holm-Sidak post-hoc test). D-G: Spontaneous locomotor activity was investigated in the open field test. There were no significant differences between groups in the tested parameters at P35. At P55, KO mice were hypoactive (D) and travelled shorter distances (E) at slower velocity (F) than WT mice. In each case, these parameters were less prominent in AAV9-MCO mice (D-F). At P55, vertical activity (G) was significantly decreased in KO and AAV9-MCO KO mice compared to WT ($^{*}P < 0.05$, Kruskal-Wallis test with Dunn's multiple comparison).

these parameters were all normalized and did not significantly differ from the WT ones.

We have previously reported a deregulation in the norepinephrine pathway in *Mecp2* KO mice (Panayotis et al., 2011; Viemari et al., 2005) and treatments targeting this pathway have proven their efficacy in alleviating breathing deficits and/or increasing survival (Bittolo et al., 2016; Roux et al., 2007; Zanella et al., 2008). In order to investigate whether the rescuing effect of the AAV9-MCO treatment could be due to a preferential improvement in the norepinephrine pathway, we examined catecholaminergic neurons of the A1C1 and A2C2 regions (Fig. 6) that can easily be identified by tyrosine hydroxylase (TH) staining (Viemari et al., 2005). In both nuclei, TH levels were lower in *Mecp2* KO mice compared to WT, but this difference reached significance in the A2C2 nucleus only. In the AAV9-MCO KO group, both nuclei showed a non-significant trend towards higher TH levels than in the KO group (Fig. 6J, K). Because other groups have shown that Mecp2 can affect bioamines levels in a cell autonomous way (Samaco et al., 2009), we examined the cellular TH levels according to the Mecp2 cell status (present/absent) in the A1C1 and A2C2 nuclei. Fig. 6L and M show that TH levels in both A1C1 and A2C2 nuclei were significantly lower in the absence of Mecp2 (Mecp2 −/TH + cells from the KO group compared to Mecp2 +/TH + from the WT group). Interestingly, in the AAV9-MCO KO mice, TH + neurons that did not express Mecp2 had significantly lower TH levels than those found in WT (Mecp2 +) TH + neurons while Mecp2 +/TH + neurons had TH levels similar to those of WT TH + neurons, which indicates a cell autonomous effect of Mecp2.

3. Discussion

It was shown that reactivation of *Mecp2* rescued adult diseased RTT mice (Guy et al., 2007; Robinson et al., 2012) which indicates that, at least in animal models, the deficits caused by a loss of *Mecp2* are reversible. Moreover, a proof-of-principle study recently showed that neonatal administration of a single-stranded AAV9 vector expressing Mecp2 was able to increase survival and rescue behavioral deficits in a mouse model of Rett syndrome (Gadalla et al., 2013; Garg et al., 2013). Together, these findings suggest that gene therapy after the disease has started might still be beneficial for RTT patients. Because RTT affects the whole CNS, direct administration of any therapeutic vector using intracerebral administration would require multiple injection sites. Although feasible

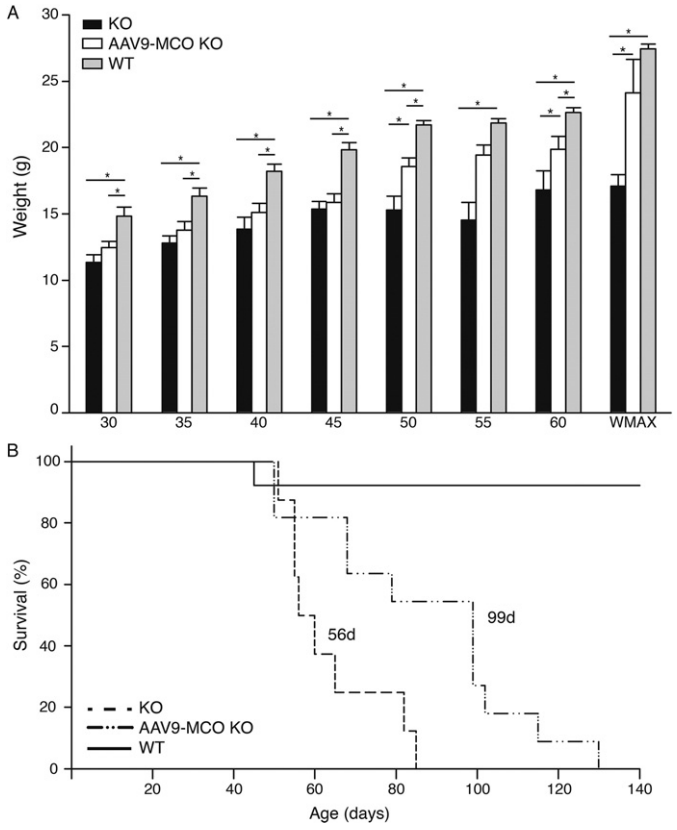

Fig. 3. Weight gain and survival are increased in AAV9-MCO KO mice. Thirty-day old *Mecp2* KO mice were intravenously administered with AAV9-MCO (AAV9-MCO KO group) and their weight (A) and survival (B) was subsequently recorded. A: *Mecp2* KO mice were significantly lighter than WT at the beginning of the study (P30, n: KO = 8, AAV9-MCO = 11, WT = 13). After AAV9-MCO injection, the treated and non-treated mice similarly gained weight up to P45 when KO mice reached a plateau while the weight of the AAV9-MCO KO kept increasing. This difference in weight reached significance at P50 and P60. Data are expressed as mean + SEM. (*$P < 0.05$, 1-way ANOVA with Holm-Sidak post-hoc test or Kruskal-Wallis one-way analysis of variance on ranks followed by Dunn's Method pairwise comparison). B: Administration of AAV9-MCO significantly extended the lifespan of *Mecp2* KO mice when compared to their untreated littermate controls ($P < 0.014$ Kaplan-Meier survival analysis AAV9-MCO KO vs KO, n: KO = 8, AAV9-MCO = 11, WT = 13). Median lifespan values (in days) are indicated on the graph.

(Leone et al., 2012), such interventions are invasive and can have serious, and sometimes lethal, consequences for the patients (Worgall et al., 2008). In addition, Rett patients are known to display a higher risk of complications after sedation (Tofil et al., 2006), which would further complicate any surgical procedure. Based on these considerations, and in keeping with translational goals, we elected the use of an intravascular approach, which is less invasive and made possible through the use of an AAV virus able to cross the BBB (Duque et al., 2009; Foust et al., 2009). In order to further optimize vector expression, we used a codon-optimized version of *Mecp2* (*MCO*) packaged in a self-complementary AAV9, two characteristics known to increase transgene expression (Raab et al., 2010) and transduction efficiency (McCarty et al., 2001), respectively. We also chose to treat 30 day-old juvenile mice, which would be closer to the age at which RTT patients are diagnosed and would become eligible for gene therapy.

After systemic administration of the AAV9-MCO to young adult *Mecp2* KO mice, we found that Mecp2 was present at 10–20% of the level observed in WT mice and observed a significant increase in survival compared to untreated *Mecp2* KO mice, which is in agreement with previous reports (Gadalla et al., 2013; Garg et al., 2013). However, unlike those studies, we did see an improvement in weight gain, a delay in behavioral deficit occurrence and a normalization of apneas in the treated AAV9-MCO KO mice. These additional phenotypical improvements could be due to the use of the *MCO* (Raab et al., 2010), which may explain the higher percentage of brain cells in which detectable Mecp2 level was found. Although the use of the *MCO* seemed to be beneficial, its higher expression could be a concern because Mecp2 needs to be tightly regulated in order to avoid overexpression and the subsequent appearance of MECP2 duplication syndrome neurological symptoms (Na et al., 2012). However, previous studies have also reported that Mecp2 expression is heterogeneous and varies throughout the mouse and human brains (LaSalle et al., 2001) and allows for some flexibility (Gadalla et al., 2013; Luikenhuis et al., 2004).

Interestingly, we noticed a higher percentage of Mecp2 + cells in posterior brain regions compared to more anterior ones. On the one hand, this increase could be due to the dense vascularization found in the brainstem (Duvernoy and Risold, 2007) that probably allowed for more widespread viral infection. On the other hand, the circumventricular organs, such as the area postrema, located at the junction between the medulla and the spinal cord, is composed of blood vessels devoid of the blood brain barrier, which could have provided the vector unhindered access to the brain. In addition, it is part of the vagal complex and is involved in cardiovascular and respiratory regulation (Dergacheva et al., 2010). The latter is of particular interest, as we showed that AAV9-MCO vector administration to *Mecp2* KO mice efficiently rescued the occurrence of severe apneas and normalized the hypoventilation and breathing variability. At the cellular level, Mecp2 expression led to the normalization of tyrosine hydroxylase (TH) levels in the A1C1 and A2C2 chatecholaminergic neurons in a cell autonomous way, which could explain the rescuing effect of AAV9-MCO on apneas. This is supported by the facts that *Mecp2* deficiency leads to a developmental decrease in TH associated to a decrease of the noradrenergic content (Panayotis et al., 2011; Roux and Villard, 2010; Roux et al., 2008) and that a deregulation of the norepinephrine pathway is involved in the breathing deficits observed in *Mecp2* deficient mice (Panayotis et al., 2011; Viemari et al., 2005). However, it is highly likely that the increase in TH levels is not the sole factor involved in the normalization of breathing defects since we also found Mecp2 expression in TH − cells. Similarly to what we observe here, we can hypothesize that other neurotransmitter pathways may have been modified, as seen in GABAergic cortical neurons (Gadalla et al., 2013) or 5HT neurons (Abdala et al., 2014). Although glia likely plays an important role in RTT neuropathology (Lioy et al., 2011), it is unlikely to explain our results because we could not detect any Mecp2 expression in astrocytes.

Given our intravascular approach and the fact that the AAV9 vector displays a high tropism for the heart and liver (Inagaki et al., 2006), the possibility of off-target effect needs to be addressed. Post-mortem observation did not reveal any gross morphology abnormality after vector administration to *Mecp2* KO mice (data not shown). While the use of an optimized *Mecp2* isoform increased the number of cells expressing detectable Mecp2 levels and improved phenotypical deficits, it also considerably increased Mecp2 expression in the liver of treated *Mecp2* KO mice compared to WT (supplementary Fig. 7), which will warrant further studies on the long-term effect of AAV9-MCO administration in the heterozygous *Mecp2* female mouse. This concern is of particular interest since Mecp2 was recently shown to affect liver metabolism (Kyle et al., 2016).

In conclusion, and to the best of our knowledge, this is the first report showing that intravascular administration of an AAV9 therapeutic construct in early symptomatic *Mecp2* KO mice improves phenotypical deficits. In addition, we also provide evidence that optimization of the viral construct is one important avenue to consider because it achieved therapeutic improvement with a low vector dose, a crucial point when considering treatments in large animals or, let's hope one day, in patients.

4. Materials and methods

4.1. Animals

The *Mecp2*-deficient mice (B6,129P2(C)-*Mecp2* tm1-1Bird) were obtained from the Jackson Laboratory (Charles River laboratories,

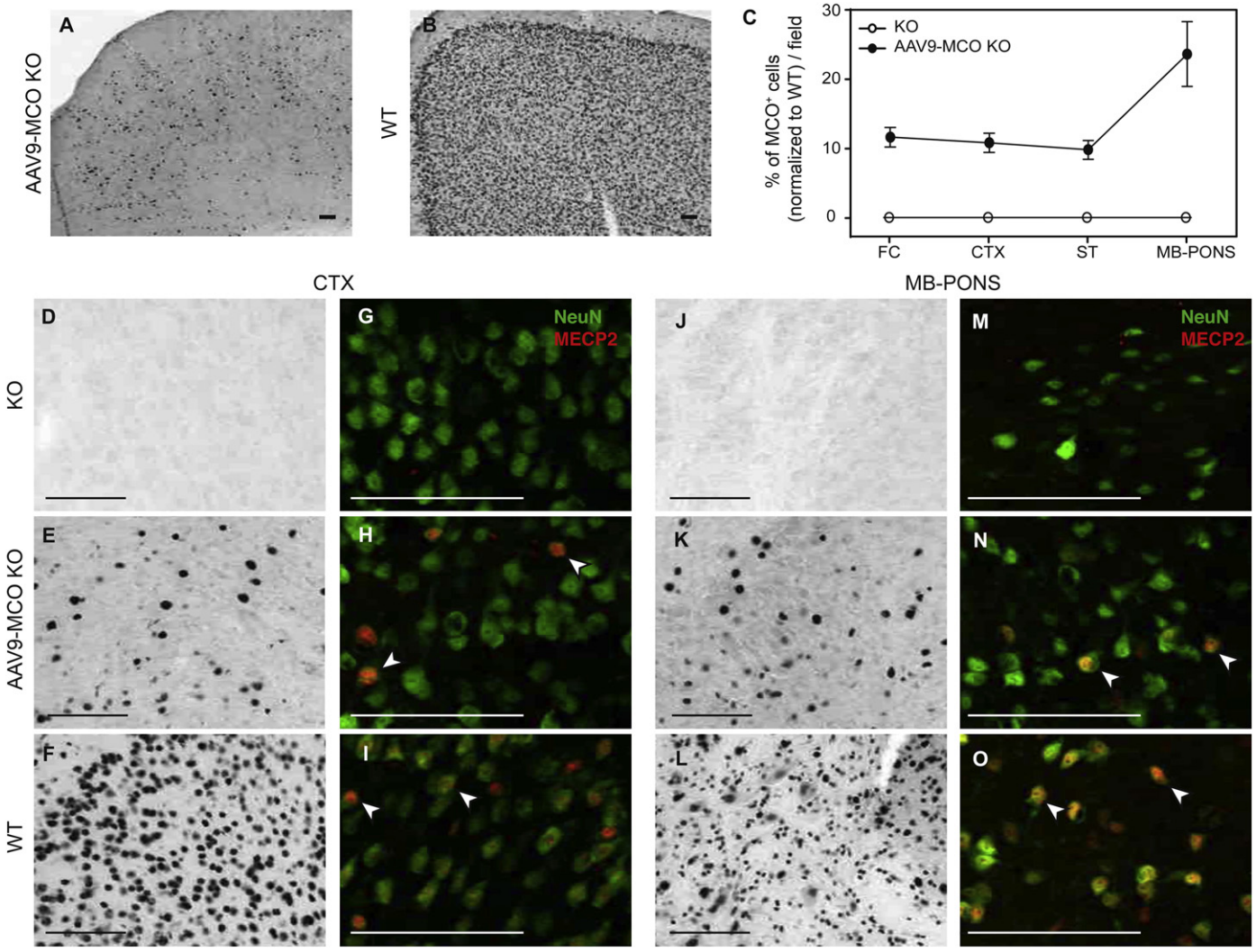

Fig. 4. AAV9-MCO administration to *Mecp2* KO mice results in low but widespread *Mecp2* expression following a rostro-caudal gradient. A, B: Example of low magnification images that were used for the semi-quantitative assessment of Mecp2 expressing (Mecp2 +) cells. Four fields/brain region (10× magnification) were processed with the ImageJ software and Mecp2+ cells were counted using the ImageJ *particle analyzing tool* (C). Data are expressed as percentage of Mecp2+ cells normalized to WT values (mean ± SEM). FC: frontal cortex, CTX: motor cortex, ST: striatum, MB-PONS: midbrain-pons region. n: KO = 4 except in CTX in which $n = 5$; AAV9-MCO = 9, WT = 11, except in FC in which $n = 10$. D-O: Representative higher magnification pictures of Mecp2+ cells in the cortex (CTX, D-I) and midbrain-pons (MB-PONS, J-O) regions from *Mecp2* KO (D, G and J, M), AAV9-MCO (E, H and K, N) and WT (F, I and L, O). In the AAV9-MCO KO (H, N) and the WT (I, O) groups, Mecp2+ cells were neurons as determined by the co-expression of Mecp2 with the NeuN neuronal marker (white arrowheads). Scale bar = 100 μm.

Chatillon-sur-Chalaronne, France) and maintained on a C57BL/6 background. Genotyping was performed by PCR-amplification following a previously described protocol (Miralvès et al., 2007). The animals were housed under a 12:12 h light / dark cycle (lights on at 07:30) and given free access to food and water. Experimental protocols were approved by the ethical committee of the Aix Marseille University and the French M.E.N.E.S.R. minister (Permit Number: 02910.02). All experiments were conducted in compliance with the European guidelines for the care and use of laboratory animals (EU directive 2010/63/EU), the *Haut Conseil des Biotechnologies* (authorization #6011) and the guide for the care and use of the laboratory animals of the French national institute for science and health (INSERM). All experiments were made to minimize animal suffering.

4.2. Plasmid design and virus preparation

4.2.1. Plasmid preparation

The *Mecp2e1* sequence was optimized by the GeneArt GeneOptimizer process (Raab et al., 2010). A plasmid (pMA-MCO) containing the inverted terminal repeats in 5′ and 3′, and flanking a transgene construct composed of the 223 bp proximal *Mecp2* promoter (−223 bp/*Pvu*II) (Adachi et al., 2005), the codon-optimized *Mecp2e1* isoform and the SV40 polyA signal was synthesized *de novo* (Geneart, Thermo Scientific, Germany). The codon-optimized Mecp2 cassette (MCO) was then excised from the pMA-MCO plasmid by *Mlu*I restriction enzyme digestion and subsequently subcloned into the intronless AAVdb plasmid backbone linearized by *Bss*HII digestion.

To generate the control vector expressing GFP, the codon-optimized *Mecp2* sequence was excised from the MCO cassette by *Nco*I-*Not*I restriction enzyme digestion and replaced by the EGFP transgene from the pEGFP-N1 vector (Clontech, Ozyme, Saint-Quentin-en-Yvelines, France) excised by the same restriction enzymes.

Plasmids were then amplified and endotoxin free DNA preparation was obtained using the EndoFree Plasmid Maxi kit (Qiagen, Courtaboeuf Cedex, France).

4.2.2. Recombinant AAV production and titration

Self-complementary recombinant pseudotyped AAV9 vectors were produced by the Vector Core at the University Hospital of Nantes

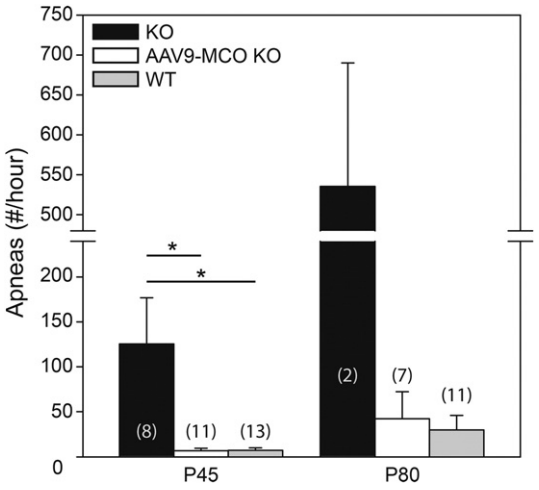

Fig. 5. AAV9-MCO administration rescues the breathing deficits in *Mecp2* KO mice: At P45, untreated *Mecp2* KO mice displayed a significantly higher number of apneas compared to the WT group. This deficit is absent in the *Mecp2* KO mice after administration of the AAV9-MCO vector (*$P < 0.05$, Kruskal-Wallis test with Dunn's multiple comparison, n: KO = 8, AAV9-MCO = 11, WT = 13). By P80, although the number of apneas in the treated *Mecp2* KO mice was similar to the WT group, the sample sizes were too small to be tested for significance (n: KO = 2, AAV9-MCO = 7, WT = 11). Data (vertical bars) are expressed as mean + SEM.

(www.atlantic-gene-therapies.fr) based on the protocol of Ayuso et al. (2010). Virus titration was performed by dot blot (Ayuso et al., 2010) and expressed as viral genome (vg)/ml.

4.3. in vivo AAV injections

4.3.1. AAV9 control vector

Four week-old wild-type (WT) male mice were sedated with a mixture of ketamine/xylazine (80 mg/kg BW and 8 mg/kg BW i.p., respectively) and intravenously injected with the AAV9-GFP vectors (5×10^9 vg/ BW) through the tail vein.

4.3.2. AAV9 experimental vector

Four week-old *Mecp2*-deficient (KO) male mice and their littermate wild-type controls were lightly sedated with a mixture of ketamine/xylazine (30 mg/kg BW and 3 mg/kg BW i.p., respectively) and intravenously injected with AAV9-MCO (1.6×10^{10} vg/g BW) or PBS only through the tail vein.

Table 1
Treatment with AAV9-MCO rescues the main breathing deficits in *Mecp2* KO mice at P45.

	KO (8)	AAV9-MCO KO (11)	WT (13)
Hyperventilation	120,401 ± 809	12,418 ± 611*	9966 ± 751
Ventilation	727 ± 227	501 ± 232+	1407 ± 378
Hypoventilation	71.2 ± 31.5	6.7 ± 3.7+	26.3 ± 16.3
Apneas	125.6 ± 62.7	6.5 ± 3.1+	7.1 ± 2.7+
Mean frequency	223 ± 6.2	213.2 ± 7.2	195.4 ± 5.5*
Variability	57.5 ± 2.4	40.9 ± 3.1***	46 ± 1.8**

Breathing was recorded by whole body plethysmography and analyzed by Spike2 interface and software (v.5.04, Cambridge Electronic Design Ltd., Cambridge, UK). Breathing cycles were divided into four groups according to their duration: hyperventilation (including cycles in the range 0–0.3 s range); ventilation (0.3–0.7 s); hypoventilation (0.7–1 s) and apneas (1–∞ s). The breathing variability was calculated as the mean standard variability. Breathing parameters were obtained from the analysis of quiet period of at least 100 consecutive cycles. +$P < 0.05$, Kruskal-Wallis test with Dunn's multiple comparison vs the *Mecp2* KO group (KO). *** $P < 0.001$, ** $P < 0.01$, * $P < 0.05$, 1-Way ANOVA with Holm-Sidak post-hoc test vs the KO group. Values are expressed as mean ± SEM. (n): number of animals/group.

4.4. Behavioral testing

All mice were weighted three times a week and assessed for survival. In order to maintain animal well-being and minimize animal suffering, humane endpoints were determined as an excessive weight loss (below 80% of maximum weight), obvious breathing distress (known to occur in *Mecp2* KO mice) or repetitive behavior ending in severe injury (over-grooming).

All mice were tested in the open field and on the accelerating rotarod at P35 and P55, and in the elevated plus maze at P45.

4.4.1. Open field

Each mouse was placed in an open field (100 cm diameter) under bright light condition (300 lx) and its exploratory behavior was recorded and processed by the Videotrack software (Viewpoint, Lyon, France). Activity and average velocity (cm/s) were determined from the total distance moved and activity duration provided by the Videotrack software. Each trial consisted of a 20 min period divided in 10 min bins during which vertical activity (leaning, rearing) was recorded by the observer.

4.4.2. Accelerating rotarod

Sensorimotor function was assessed in mice with the accelerating rotarod apparatus (Panlab LE-8200, Harvard Apparatus). Each trial lasted 5 min maximum, starting at 4 rpm and increasing by 1 rpm every 8 s until it reached the maximum speed of 40 rpm. Mice were given 3 consecutive trials, with 5 min rest periods in between. Latency to fall (in seconds) was recorded and the highest time was recorded. In the case of mice clinging to the rod, the trial was stopped and the passive rotation was considered a failure in performance like falling (Brown et al., 2005).

4.4.3. Elevated plus maze

Anxiety-related behavior was assessed using the elevated plus maze (70 lx). The maze (Med Associates Inc., St Albans, VT, USA) consisted of two walled areas (safe environment) and two open areas (anxiety-provoking environment), identical in length (35 cm). Each mouse was placed in the center part of the maze and allowed free access for 10 min (2×5 min bins). The number of center platform crossings and the length of time spent in the open arms, indicative of activity and anxiety level, respectively, were manually recorded.

4.5. Whole body plethysmography

Breathing was recorded in 45 day-old *Mecp2* KO mice and their wild-type littermate controls, as reported previously (Roux et al., 2007; Viemari et al., 2005). Briefly, each unrestrained mouse was placed in a clear Plexiglas chamber composed of an animal and reference chambers (200 ml and 100 ml capacity, respectively). The pressure difference between the animal and reference chambers was recorded, amplified, filtered and fed to an analog-to-digital converter (sampling frequency 1 kHz). The data was stored and analyzed by the Spike2 interface and software (v.5.04, Cambridge Electronic Design Ltd., Cambridge, UK). Animals were given at least 30 min to acclimate to the chamber before recording was started and analysis only included periods during which the animals were quiet. Breathing cycles were divided into four groups according to their duration: hyperventilation (including cycles in the range 0–0.3 s range); ventilation (0.3–0.7 s); hypoventilation (0.7–1 s) and apneas (1–∞ s). The breathing variability was calculated as the mean standard variability. Breathing parameters were obtained from the analysis of quiet period of at least 100 consecutive cycles.

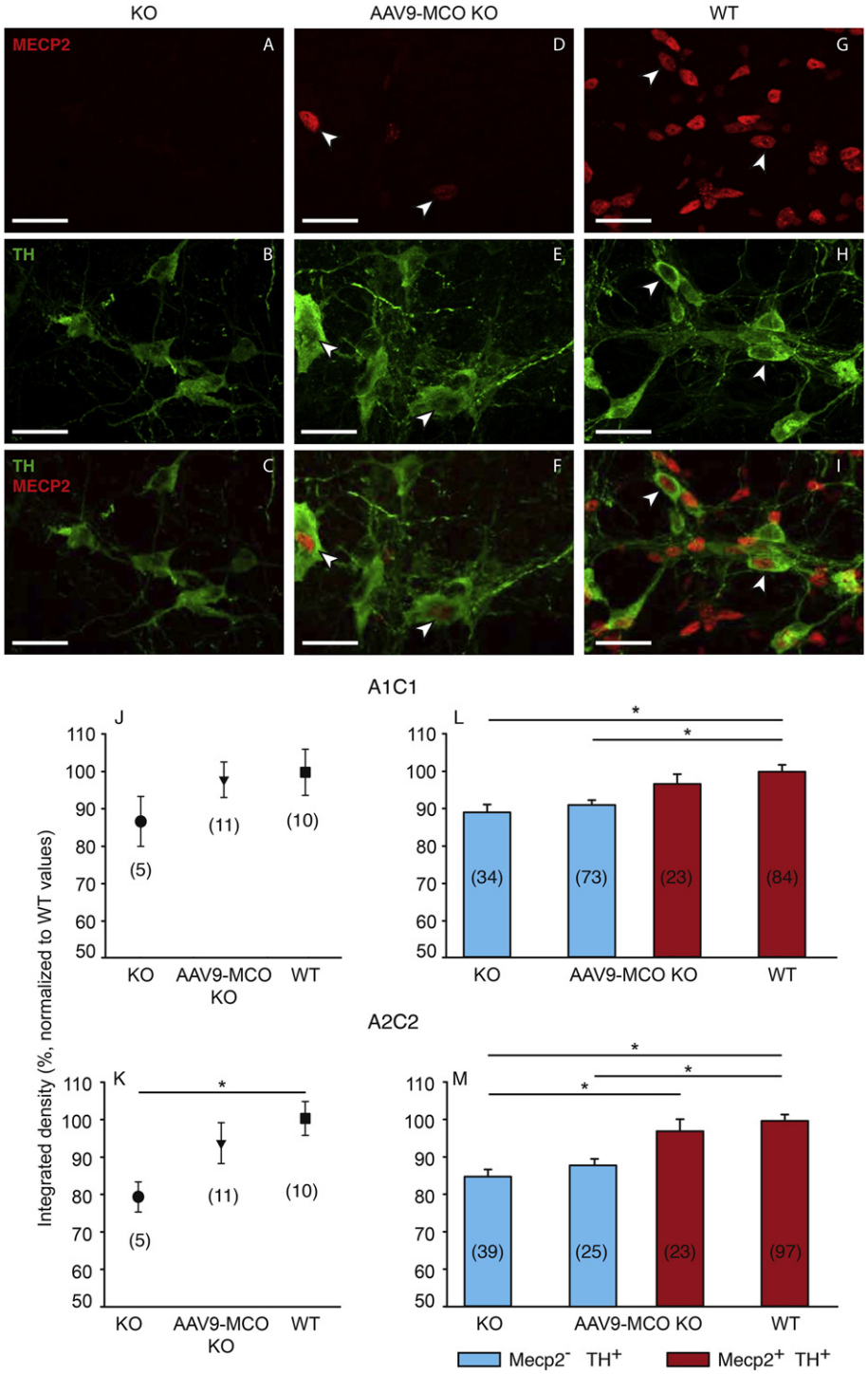

Fig. 6. AAV9-MCO administration increases TH levels in the A1C1 and A2C2 nuclei in a cell autonomous way. A-I: Representative images showing the expression of Mecp2 (in red) in the A1C1 tyrosine hydroxylase expressing neurons (TH+, in green) in Mecp2 KO (A-C), AAV9-MCO KO (D-F) and WT groups (G-I). Examples of TH+ neurons co-expressing Mecp2 are indicated by white arrowheads. Scale bar = 25 μm. J-M: The semi-quantitative assessment of TH fluorescent intensity in A1C1 and A2C2 nuclei (J and K, respectively) or individual catecholaminergic neurons (at least 5 TH+ cells/animal in each group, L and M, respectively) shows that Mecp2 expression increases TH levels in a cell autonomous manner. The integrated values were obtained for each individual neuron and analyzed according to the present/absent (+ or -) Mecp2 cell status. *$P < 0.05$, Kruskal-Wallis test with Dunn's multiple comparison. Group size (n) is shown in parenthesis and corresponds to the number of animals/group (J, K) or to the number of neurons/group (L, M).

4.6. Animal perfusion and Immunostaining

Animals were euthanized with an overdose of sodium pentobarbital (100 mg/kg BW, Ceva Santé Animale, La Ballastiere, France) and transcardially perfused with PBS 1X (Sigma-Aldrich, Saint-Quentin Fallavier, France) followed by a solution of 4% parafomaldehyde (PFA, Sigma-Aldrich) in PBS 1X. The brain, and peripheral organs (liver, heart, spleen and kidney) were dissected and post-fixed overnight in 4% PFA-PBS at 4C. After 48 h in a 20% sucrose-PBS 1X solution, brains and peripheral organs were embedded in Tissue-Tek CRYO-OCT compound (Fisher Scientific, Illkirch, France) and serially sectioned at 40 μm thickness on a Leica cryostat (VT1200s, Leica, Nanterre, France).

Sections were kept at 4C in cryoprotectant solution (30% sucrose, 30% ethylene glycol, 1% Polyvinylpyrrolidone 40 in 0.1 M phosphate buffer) until processed for immunostaining.

4.6.1. Immunohistochemistry

After washing in potassium phosphate-buffered saline (KPBS) buffer (0.02 M, pH 7.4, 4 × 10 min), brain sections were incubated for 30 min in KPBS-1% hydrogen peroxide (Sigma-Aldrich, Saint-Quentin Fallavier, France) in order to block endogenous peroxidases. After 3 washed in KPBS, sections were incubated for 1 h at room temperature in blocking solution (2% normal donkey serum [Jackson ImmunoReasearch Europe, Ltd., Suffolk, UK], 0.5% Triton X-100, 0.02 M KPBS). Sections were then incubated with the primary antibody (rabbit anti-Mecp2, #3456, 1:500; Cell Signaling Technologies, Ozyme, St-Quentin-En-Yvelines, France or goat anti-GFP, #ab6673, 1:500; Abcam, Cambridge, United Kingdom) diluted in blocking solution or in blocking solution only (negative control) for 48 h at 4C under constant agitation. After washing four times in 0.02 mM KPBS, sections were incubated 1 h in secondary antibody diluted at 1:200 in blocking solution (biotinylated donkey anti-goat IgG, #sc-2042 or anti-rabbit IgG, #sc2089; Santa Cruz Biotechnologies Inc., Heidelberg, Germany). Secondary amplification and detection were performed using the VectaStain ABC Elite Kit (#PK-6101; Vector Labs, Eurobio, Courtaboeuf, France) and the Vector VIP Peroxidase (HRP) Substrate Kit (#SK-4600) that were used according to the manufacturer recommendation. Immunostained sections were mounted on SuperFrost Plus slides (Fisher Scientific), dehydrated in ethanol (successive baths in 50%, 75%, 95% and 100% ethanol), cleared in Xylene and mounted in DPX mounting media (Fisher Scientific). Pictures were taken at 10× and 20× magnification on a BX51 Olympus microscope (Olympus, Rungis, France).

4.6.2. Immunohistofluorescence

Sections were washed in KPBS 0.02 M for four times, incubated in blocking solution (as described above) for 1 h and transferred in primary antibody solution or in blocking solution only (negative control sections) for 48 h at 4 °C. After washing the sections four times for 10 min, they were incubated for 1 h at room temperature with the secondary antibody diluted in blocking solution and then washed four more times in KPBS. Sections were then mounted on glass slides, air-dried for 30 min and coverslipped with Shandon Immu-Mount (ThermoFisher Scientific). Primary antibodies were as follows: goat anti-GFP, (#ab6673, 1:500; Abcam), rabbit anti-Mecp2 (#3456, 1:500; CST), mouse anti-Mecp2 (#M7443, 1:200; Sigma-Aldrich), rabbit anti-NeuN (1:1500, #ab104225; Abcam), sheep anti-TH (1:500, MAB1542, Chemicon, Millipore). Secondary antibodies were bought from ThermoFisher Scientific and were all raised in donkey, they were: anti-goat Alexa 488 (1:500, #A11055), anti-goat Alexa 555 (1:400, #A21432), anti-rabbit Alexa 596 (#R37117), anti-rabbit Fluoprobe 488 (1:400, FP-SA5110, Interchim, Montluçon, France), anti-rabbit Fluoprobe 547 (1:400, FP-SB4110, Interchim).

Pictures were taken at 20× and 40× magnification on a Zeiss Apotome microscope (Carl Zeiss Microimaging, Jena, Germany). Exposition times, images processing and merging were done using the same parameter within each experiment.

4.7. Image quantification

4.7.1. TH Immunoquantification

Semi-quantitative assessment of TH expression was carried out as previously described (Roux et al., 2008; Roux et al., 2010). Briefly, the immunolabelled slides were digitized and recorded using a Leica DMR microscope (Leica Microsystems, Wetzlar, Germany) equipped with a CoolSNAP camera (Princeton, Trenton, NJ, USA). To minimize inter-individual variability, immunostaining was carried out at once and pictures of specific brain region were taken during the same session. For each session, the first slice scanned at the beginning of a single day was scanned again at the end in order to assess any change in light intensity. In addition, the linearity of the camera response was checked, the level of fluorescence intensity was carefully chosen in order to never reach saturation and, once set, never changed throughout the session. All pictures were converted in grayscale (8-bit images). Densitometric analysis (integrated density) of the staining was performed using the ImageJ software from the National Institutes of Health (http://rsb.info.nih.gov). The Optical density was calculated as OD = log 10 (255/luminance). The TH staining level of Mecp2 + and Mecp2 − cells was measured in at least 5 cells/animal. For each section, we subtracted the mean of the specific staining (TH +) by the mean of the background (TH −).

4.7.2. GFP and Mecp2 immunoquantification

Sections were visualized with a Microvision Instruments apparatus (Evry, France) composed of an Olympus microscope BX51 with a SCAN^{plus} motorized platform and coupled to a Sony Digital Interface camera (XCG-U100CR). Anterior (FC, CTX, ST) and posterior (MB, MB-Pons) brain areas were imaged with the Histolab software (v.8.1.1, Microvision Instruments) at a 10× magnification. Each brain location was carefully selected and at least 4 fields /brain area (2 on each side) of the same surface in each group was used for analysis.

4.7.2.1. GFP immunoquantification. Because the AAV9-CMV-GFP vector transduced both neurons and astrocytes (Fig. 1 and suppl Fig. 1), GFP expressing (GFP +) cells lacked uniformity and automated cell counting was not recommended. GFP + cells were therefore manually counted using thresholded images (default parameters, Fiji schindelin (Schindelin et al., 2012)) and counted cells were grouped into neuronal and non-neuronal subtypes based on their morphology (presence of axon and/or dendrites in neuron-like cells).

4.7.2.2. Mecp2 immunoquantification. Using the Fiji software, images were converted to 8-bit format, then thresholded, and a region of interest (ROI) was drawn on the image. The number of particle in the ROI was then counted with the Fiji *particle analyzing tool.* All slides were analyzed with the experimenter blind for genotype and for the treatment.

4.8. Statistical analysis

All statistical analyses were performed using SigmaPlot 11 (Systat Software Inc., San Jose, CA). Comparison between 2 groups was analyzed by a Mann-Whitney U statistics test. Genotype differences were analyzed using a one-way ANOVA (normal distribution, equal variance) followed by the Holm-Sidak post-hoc tests or the Kruskal-Wallis one-way analysis of variance on ranks followed by Dunn's Method pairwise comparison procedure when the normality test failed. Data are expressed as means ± SEM and $P < 0.05$ was considered significant for all tests.

Funding

This work was supported by INSERM, Aix Marseille University, grants from the AFM-Téléthon (Strategic pole MNH Decrypt) and Association Française du Syndrome de Rett (AFSR).

Acknowledgements

We thank the Vector Core (www.atlantic-gene-therapies.fr) at the University Hospital of Nantes for the rAAV vector production, Christophe Scajola and Adeline Spiga Ghata for expert animal care and Pascal Weber for microscopy assistance.

Appendix A. Supplementary data

Supplementary data to this article can be found online at http://dx.doi.org/10.1016/j.nbd.2016.12.009.

References

Abdala, A.P., Lioy, D.T., Garg, S.K., Knopp, S.J., Paton, J.F., Bissonnette, J.M., 2014. Effect of Sarizotan, a 5-HT1a and D2-like receptor agonist, on respiration in three mouse models of Rett syndrome. Am. J. Respir. Cell Mol. Biol. 50:1031–1039. http://dx.doi.org/10.1165/rcmb.2013-0372OC.

Adachi, M., Keefer, E.W., Jones, F.S., 2005. A segment of the Mecp2 promoter is sufficient to drive expression in neurons. Hum. Mol. Genet. 14:3709–3722. http://dx.doi.org/10.1093/hmg/ddi402.

Amir, R.E., Van den Veyver, I.B., Wan, M., Tran, C.Q., Francke, U., Zoghbi, H.Y., 1999. Rett syndrome is caused by mutations in X-linked MECP2, encoding methyl-CpG-binding protein 2. Nat Genet 23:185–188. http://dx.doi.org/10.1038/13810.

Asokan, A., Schaffer, D.V., Samulski, R.J., 2012. The AAV vector toolkit: poised at the clinical crossroads. Mol. Ther. 20:699–708. http://dx.doi.org/10.1038/mt.2011.287.

Ayuso, E., Mingozzi, F., Bosch, F., 2010. Production, purification and characterization of adeno-associated vectors. Curr. Gene Ther. 10, 423–436.

Bittolo, T., Raminelli, C.A., Deiana, C., Baj, G., Vaghi, V., Ferrazzo, S., Bernareggi, A., Tongiorgi, E., 2016. Pharmacological treatment with mirtazapine rescues cortical atrophy and respiratory deficits in MeCP2 null mice. Sci. Rep. 6:19796. http://dx.doi.org/10.1038/srep19796.

Brown, S.D., Chambon, P., de Angelis, M.H., Eumorphia Consortium, 2005. EMPReSS: standardized phenotype screens for functional annotation of the mouse genome. Nat. Genet. 37:1155. http://dx.doi.org/10.1038/ng1105-1155.

Dergacheva, O., Griffioen, K.J., Neff, R.A., Mendelowitz, D., 2010. Respiratory modulation of premotor cardiac vagal neurons in the brainstem. Respir. Physiol. Neurobiol. 174: 102–110. http://dx.doi.org/10.1016/j.resp.2010.05.005.

Dragich, J.M., Kim, Y.H., Arnold, A.P., Schanen, N.C., 2007. Differential distribution of the MeCP2 splice variants in the postnatal mouse brain. J. Comp. Neurol. 501:526–542. http://dx.doi.org/10.1002/cne.21264.

Dufour, B.D., Smith, C.A., Clark, R.L., Walker, T.R., McBride, J.L., 2014. Intrajugular vein delivery of AAV9-RNAi prevents neuropathological changes and weight loss in Huntington's disease mice. Mol. Ther. 22:797–810. http://dx.doi.org/10.1038/mt.2013.289.

Duque, S., Joussemet, B., Riviere, C., Marais, T., Dubreil, L., Douar, A.M., Fyfe, J., Moullier, P., Colle, M.A., Barkats, M., 2009. Intravenous administration of self-complementary AAV9 enables transgene delivery to adult motor neurons. Mol. Ther. 17:1187–1196. http://dx.doi.org/10.1038/mt.2009.71.

Duvernoy, H.M., Risold, P.Y., 2007. The circumventricular organs: an atlas of comparative anatomy and vascularization. Brain Res. Rev. 56:119–147. http://dx.doi.org/10.1016/j.brainresrev.2007.06.002.

Foust, K.D., Nurre, E., Montgomery, C.L., Hernandez, A., Chan, C.M., Kaspar, B.K., 2009. Intravascular AAV9 preferentially targets neonatal neurons and adult astrocytes. Nat. Biotechnol. 27:59–65. http://dx.doi.org/10.1038/nbt.1515.

Gadalla, K.K., Bailey, M.E., Spike, R.C., Ross, P.D., Woodard, K.T., Kalburgi, S.N., Bachaboina, L., Deng, J.V., West, A.E., Samulski, R.J., Gray, S.J., Cobb, S.R., 2013. Improved survival and reduced phenotypic severity following AAV9/MECP2 gene transfer to neonatal and juvenile male Mecp2 knockout mice. Mol. Ther. 21:18–30. http://dx.doi.org/10.1038/mt.2012.200.

Garg, S.K., Lioy, D.T., Cheval, H., McGann, J.C., Bissonnette, J.M., Murtha, M.J., Foust, K.D., Kaspar, B.K., Bird, A., Mandel, G., 2013. Systemic delivery of MeCP2 rescues behavioral and cellular deficits in female mouse models of Rett syndrome. J. Neurosci. 33: 13612–13620. http://dx.doi.org/10.1523/JNEUROSCI.1854-13.2013.

Gray, S.J., Foti, S.B., Schwartz, J.W., Bachaboina, L., Taylor-Blake, B., Coleman, J., Ehlers, M.D., Zylka, M.J., McCown, T.J., Samulski, R.J., 2011a. Optimizing promoters for recombinant adeno-associated virus-mediated gene expression in the peripheral and central nervous system using self-complementary vectors. Hum. Gene Ther. 22: 1143–1153. http://dx.doi.org/10.1089/hum.2010.245.

Gray, S.J., Matagne, V., Bachaboina, L., Yadav, S., Ojeda, S.R., Samulski, R.J., 2011b. Preclinical differences of intravascular AAV9 delivery to neurons and glia: a comparative study of adult mice and nonhuman primates. Mol. Ther. 19:1058–1069. http://dx.doi.org/10.1038/mt.2011.72.

Guy, J., Gan, J., Selfridge, J., Cobb, S., Bird, A., 2007. Reversal of neurological defects in a mouse model of Rett syndrome. Science 315:1143–1147. http://dx.doi.org/10.1126/science.1138389.

Guy, J., Hendrich, B., Holmes, M., Martin, J.E., Bird, A., 2001. A mouse Mecp2-null mutation causes neurological symptoms that mimic Rett syndrome. Nat. Genet. 27:322–326. http://dx.doi.org/10.1038/85899.

Hagberg, B., 1995. Rett syndrome: clinical peculiarities and biological mysteries. Acta Paediatr. 84, 971–976.

Inagaki, K., Fuess, S., Storm, T.A., Gibson, G.A., Mctiernan, C.F., Kay, M.A., Nakai, H., 2006. Robust systemic transduction with AAV9 vectors in mice: efficient global cardiac gene transfer superior to that of AAV8. Mol. Ther. 14:45–53. http://dx.doi.org/10.1016/j.ymthe.2006.03.014.

Julu, P.O., Kerr, A.M., Hansen, S., Apartopoulos, F., Jamal, G.A., 1997. Immaturity of medullary cardiorespiratory neurones leading to inappropriate autonomic reactions as a likely cause of sudden death in Rett's syndrome. Arch. Dis. Child. 77, 464–465.

Katz, D.M., Berger-Sweeney, J.E., Eubanks, J.H., Justice, M.J., Neul, J.L., Pozzo-Miller, L., Blue, M.E., Christian, D., Crawley, J.N., Giustetto, M., Guy, J., Howell, C.J., Kron, M., Nelson, S.B., Samaco, R.C., Schaevitz, L.R., St Hillaire-Clarke, C., Young, J.L., Zoghbi, H.Y., Mamounas, L.A., 2012. Preclinical research in Rett syndrome: setting the foundation for translational success. Dis. Model. Mech. 5:733–745. http://dx.doi.org/10.1242/dmm.011007.

Katz, D.M., Dutschmann, M., Ramirez, J.M., Hilaire, G., 2009. Breathing disorders in Rett syndrome: progressive neurochemical dysfunction in the respiratory network after birth. Respir. Physiol. Neurobiol. 168:101–108. http://dx.doi.org/10.1016/j.resp.2009.04.017.

Kerr, A.M., Armstrong, D.D., Prescott, R.J., Doyle, D., Kearney, D.L., 1997. Rett syndrome: analysis of deaths in the British survey. Eur. Child Adolesc. Psychiatry 6 (Suppl. 1), 71–74.

Kyle, S.M., Saha, P.K., Brown, H.M., Chan, L.C., Justice, M.J., 2016. MeCP2 co-ordinates liver lipid metabolism with the NCoR1/HDAC3 corepressor complex. Hum. Mol. Genet. http://dx.doi.org/10.1093/hmg/ddw156.

LaSalle, J.M., Goldstine, J., Balmer, D., Greco, C.M., 2001. Quantitative localization of heterogeneous methyl-CpG-binding protein 2 (MeCP2) expression phenotypes in normal and Rett syndrome brain by laser scanning cytometry. Hum. Mol. Genet. 10, 1729–1740.

Leone, P., Shera, D., McPhee, S.W., Francis, J.S., Kolodny, E.H., Bilaniuk, L.T., Wang, D.J., Assadi, M., Goldfarb, O., Goldman, H.W., Freese, A., Young, D., During, M.J., Samulski, R.J., Janson, C.G., 2012. Long-term follow-up after gene therapy for canavan disease. Sci. Transl. Med. 4:165ra163. http://dx.doi.org/10.1126/scitranslmed.3003454.

Lioy, D.T., Garg, S.K., Monaghan, C.E., Raber, J., Foust, K.D., Kaspar, B.K., Hirrlinger, P.G., Kirchhoff, F., Bissonnette, J.M., Ballas, N., Mandel, G., 2011. A role for glia in the progression of Rett's syndrome. Nature 475:497–500. http://dx.doi.org/10.1038/nature10214.

Lombardi, L.M., Baker, S.A., Zoghbi, H.Y., 2015. MECP2 disorders: from the clinic to mice and back. J. Clin. Invest. 125:2914–2923. http://dx.doi.org/10.1172/JCI78167.

Luikenhuis, S., Giacometti, E., Beard, C.F., Jaenisch, R., 2004. Expression of MeCP2 in postmitotic neurons rescues Rett syndrome in mice. Proc. Natl. Acad. Sci. U. S. A. 101:6033–6038. http://dx.doi.org/10.1073/pnas.0401626101.

Lyst, M.J., Bird, A., 2015. Rett syndrome: a complex disorder with simple roots. Nat. Rev. Genet. 16:261–275. http://dx.doi.org/10.1038/nrg3897.

McCarty, D.M., Monahan, P.E., Samulski, R.J., 2001. Self-complementary recombinant adeno-associated virus (scAAV) vectors promote efficient transduction independently of DNA synthesis. Gene Ther. 8:1248–1254. http://dx.doi.org/10.1038/sj.gt.3301514.

Meehan, R.R., Lewis, J.D., Bird, A.P., 1992. Characterization of MeCP2, a vertebrate DNA binding protein with affinity for methylated DNA. Nucleic Acids Res. 20, 5085–5092.

Miralvès, J., Magdeleine, E., Joly, E., 2007. Design of an improved set of oligonucleotide primers for genotyping MeCP2tm1.1Bird KO mice by PCR. Mol. Neurodegener. 2:16. http://dx.doi.org/10.1186/1750-1326-2-16.

Na, E.S., Nelson, E.D., Adachi, M., Autry, A.E., Mahgoub, M.A., Kavalali, E.T., Monteggia, L.M., 2012. A mouse model for MeCP2 duplication syndrome: MeCP2 overexpression impairs learning and memory and synaptic transmission. J. Neurosci. 32:3109–3117. http://dx.doi.org/10.1523/JNEUROSCI.6000-11.2012.

Naidu, S., 1997. Rett syndrome: a disorder affecting early brain growth. Ann. Neurol. 42: 3–10. http://dx.doi.org/10.1002/ana.410420104.

Neul, J.L., Kaufmann, W.E., Glaze, D.G., Christodoulou, J., Clarke, A.J., Bahi-Buisson, N., Leonard, H., Bailey, M.E., Schanen, N.C., Zappella, M., Renieri, A., Huppke, P., Percy, A.K., RettSearch Consortium, 2010. Rett syndrome: revised diagnostic criteria and nomenclature. Ann Neurol 68:944–950. http://dx.doi.org/10.1002/ana.22124.

Panayotis, N., Pratte, M., Borges-Correia, A., Ghata, A., Villard, L., Roux, J.C., 2011. Morphological and functional alterations in the substantia nigra pars compacta of the Mecp2-null mouse. Neurobiol. Dis. 41:385–397. http://dx.doi.org/10.1016/j.nbd.2010.10.006.

Pelka, G.J., Watson, C.M., Radziewic, T., Hayward, M., Lahooti, H., Christodoulou, J., Tam, P.P., 2006. Mecp2 deficiency is associated with learning and cognitive deficits and altered gene activity in the hippocampal region of mice. Brain 129:887–898. http://dx.doi.org/10.1093/brain/awl022.

Raab, D., Graf, M., Notka, F., Schödl, T., Wagner, R., 2010. The GeneOptimizer algorithm: using a sliding window approach to cope with the vast sequence space in multiparameter DNA sequence optimization. Syst. Synth. Biol. 4:215–225. http://dx.doi.org/10.1007/s11693-010-9062-3.

Robinson, L., Guy, J., McKay, L., Brockett, E., Spike, R.C., Selfridge, J., De Sousa, D., Merusi, C., Riedel, G., Bird, A., Cobb, S.R., 2012. Morphological and functional reversal of phenotypes in a mouse model of Rett syndrome. Brain 135:2699–2710. http://dx.doi.org/10.1093/brain/aws096.

Roux, J.C., Panayotis, N., Dura, E., Villard, L., 2010. Progressive noradrenergic deficits in the locus coeruleus of Mecp2 deficient mice. J. Neurosci. Res. 88:1500–1509. http://dx.doi.org/10.1002/jnr.22312.

Roux, J., Villard, L., 2010. Biogenic amines in Rett syndrome: the usual suspects. Behav. Genet. 40:59–75. http://dx.doi.org/10.1007/s10519-009-9303-y.

Roux, J.C., Dura, E., Moncla, A., Mancini, J., Villard, L., 2007. Treatment with desipramine improves breathing and survival in a mouse model for Rett syndrome. Eur. J. Neurosci. 25:1915–1922. http://dx.doi.org/10.1111/j.1460-9568.2007.05466.x.

Roux, J.C., Dura, E., Villard, L., 2008. Tyrosine hydroxylase deficit in the chemoafferent and the sympathoadrenergic pathways of the Mecp2 deficient mouse. Neurosci. Lett. 447: 82–86. http://dx.doi.org/10.1016/j.neulet.2008.09.045.

Samaco, R.C., Mandel-Brehm, C., Chao, H.T., Ward, C.S., Fyffe-Maricich, S.L., Ren, J., Hyland, K., Thaller, C., Maricich, S.M., Humphreys, P., Greer, J.J., Percy, A., Glaze, D.G., Zoghbi, H.Y., Neul, J.L., 2009. Loss of MeCP2 in aminergic neurons causes cell-autonomous defects in neurotransmitter synthesis and specific behavioral abnormalities. Proc. Natl. Acad. Sci. U. S. A. 106:21966–21971. http://dx.doi.org/10.1073/pnas.0912257106.

Samaco, R.C., Neul, J.L., 2011. Complexities of Rett syndrome and MeCP2. J. Neurosci. 31: 7951–7959. http://dx.doi.org/10.1523/JNEUROSCI.0169-11.2011.

Schindelin, J., Arganda-Carreras, I., Frise, E., Kaynig, V., Longair, M., Pietzsch, T., Preibisch, S., Rueden, C., Saalfeld, S., Schmid, B., Tinevez, J.Y., White, D.J., Hartenstein, V., Eliceiri, K., Tomancak, P., Cardona, A., 2012. Fiji: an open-source platform for biological-image analysis. Nat. Methods 9:676–682. http://dx.doi.org/10.1038/nmeth.2019.

Tofil, N.M., Buckmaster, M.A., Winkler, M.K., Callans, B.H., Islam, M.P., Percy, A.K., 2006. Deep sedation with propofol in patients with Rett syndrome. J. Child Neurol. 21, 857–860.

Viemari, J.C., Roux, J.C., Tryba, A.K., Saywell, V., Burnet, H., Peña, F., Zanella, S., Bévengut, M., Barthelemy-Requin, M., Herzing, L.B., Moncla, A., Mancini, J., Ramirez, J.M.,

Villard, L., Hilaire, G., 2005. Mecp2 deficiency disrupts norepinephrine and respiratory systems in mice. J. Neurosci. 25:11521–11530. http://dx.doi.org/10.1523/JNEUROSCI.4373-05.2005.

Worgall, S., Sondhi, D., Hackett, N.R., Kosofsky, B., Kekatpure, M.V., Neyzi, N., Dyke, J.P., Ballon, D., Heier, L., Greenwald, B.M., Christos, P., Mazumdar, M., Souweidane, M.M., Kaplitt, M.G., Crystal, R.G., 2008. Treatment of late infantile neuronal ceroid lipofuscinosis by CNS administration of a serotype 2 adeno-associated virus expressing CLN2 cDNA. Hum. Gene Ther. 19:463–474. http://dx.doi.org/10.1089/hum.2008.022.

Zanella, S., Mebarek, S., Lajard, A.M., Picard, N., Dutschmann, M., Hilaire, G., 2008. Oral treatment with desipramine improves breathing and life span in Rett syndrome mouse model. Respir. Physiol. Neurobiol. 160:116–121. http://dx.doi.org/10.1016/j.resp.2007.08.009.